THEORETICAL ASPECTS IN RF-SUPERCONDUCTIVITY

J. Halbritter

Kernforschungszentrum Karlsruhe
Institut für Kernphysik
P.B. 3640
7500 Karlsruhe
Federal Republic of Germany.

I. INTRODUCTION

As indicated in the title "theoretical aspects", there exists not a well defined theory on rf superconductivity, but several aspects which have been connected using the limited knowledge on: dirty surfaces ,oxides, oxide - metal interfaces, inhomogeneities adjacent to such interfaces and superconducting interaction adjacent to such interfaces. All these aspects cannot be discussed in length in one paper. So we concentrate on Nb and on aspects, where new experimental and theoretical results exist.

Aspects mentioned shortly are:

Part. II : Stoechiometry of Nb-Nb_2O_5-sorption layers
Part III : BCS surface resistance $R_{BCS}(T,\omega)$
Part IV : Residual rf losses R_{resE} and R_{resH}
Part V : Deviations from thermal equilibrium
Part VI : Rf breakdown

In Part VII the electron emission out of excited states will be discussed, which is the basis of understanding of secondary- and rf field-emission of Nb cavities. With this knowledge in Part VIII multipactor - and field emission loading of superconducting Nb cavities will be analyzed.

II. STOECHIOMETRY OF Nb-Nb_2O_5-SORPTION LAYERS AND THEIR ELECTRONIC STATES

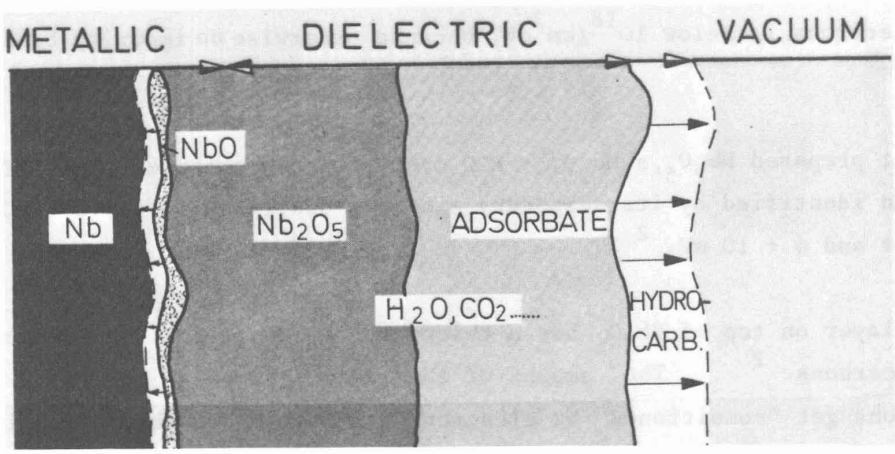

Fig. 1: Sketch of a niobium - niobium oxide - adsorbate surface region. Thicker (≃1.5nm) H_2O sorption layers may exist on not extensively pumped or heated Nb. On fresh Nb_2O_5, H_2O forms a chemisorption state which is positively charged by enhanced electron emission. By electron impact additional hydrocarbons get adsorbed (→) and polymerized. These hydrocarbons get charged negatively by electron absorption.

Destruction free XPS measurements [1,2] gave the picture of Nb surfaces shown in Fig. 1, where the following points have to be added: Beside dissolved H, O, C or Ta from the supplier or from the treatment, the Nb matrix adjacent to the surface shows Nb suboxide precipitates with $T_c^{*} \simeq 7K$. [3] These precipitates seem to be due to the oxidation of Nb, and their concentration grows with enforced oxidation, e.g. by anodizing or by electron impact. [3] The volume concentration of these suboxide ($\simeq NbO_{0.02}$) in the penetration region ($\sim$ 50 nm) is about 10% and has drastic effects on the surface impedance - see Part III - and rf breakdown - see Part VI.

The $Nb-Nb_2O_5$ interface is far from being ideal, e.g., at 4.2 K only 2% of the surface shows surface superconductivity, [5] which in addition disappears above 7 K; [3] and the conduction electrons hybridize with localized states in the oxide, which have been found by AES (Fig. 1) 2 nm deep inside the Nb_2O_5. [1] These deviations yielding states inside the energy gap shown in Fig. 2, are due to the above mentioned suboxides and due to the interface states acting pair weakening. [6] Beside acting pair weakening on the superconducting state, these interface state cause also: - Diffuse surface scattering; - Rf residual losses as summarized in Part 4; - Smearing out the transition metal - dielectric oxide as simulated by a tipped potential barrier as transition from Nb to Nb_2O_5. [7]

About 2nm on top of the Nb, the dielectric behavior of Nb_2O_5 is given by $\varepsilon_r = 36$. [7] The conduction band starts about 0.2 eV [7] above the Fermi energy, which is pinned by oxygen vacancies. The width of the conduction band is about 10 eV as shown [2] by the true secondary electron distribution reaching up to about 6 eV above the work function ϕ - see Fig. 3. The density of the oxygen vacancies, which are populated by 2 electrons, is below $10^{18}/cm^3 eV$, because otherwise an impurity band would exist.

On top of wet prepared Nb_2O_5, a $Nb_2O_5 - H_2O$ chemisorption state exists. [2] This state has been identified by its secondary electron distribution curve (EDC), which peaks around ϕ and ϕ + 10 eV. [2]

The sorption layer on top of Nb_2O_5 has a thickness between 1 and 3 nm and contains H_2O and hydrocarbons. [2] The amount of the latter grows with electron impact. [2] The hydrocarbons get "conditioned" by electron or x-ray impact showing up in an enhanced absorption (relaxation) of slow electrons. [2]

Large amounts ($\simeq$1.5 nm) of H_2O adsorbed on top of Nb_2O_5 may reduce the work function by 1 to 2 eV shown by assymetric I-U-tunnel-characteristics. [8] This thick H_2O layer is easily pumped away and so the XPS measurements [1,2] show a thin H_2O layer ($\simeq$0.5 nm) only.

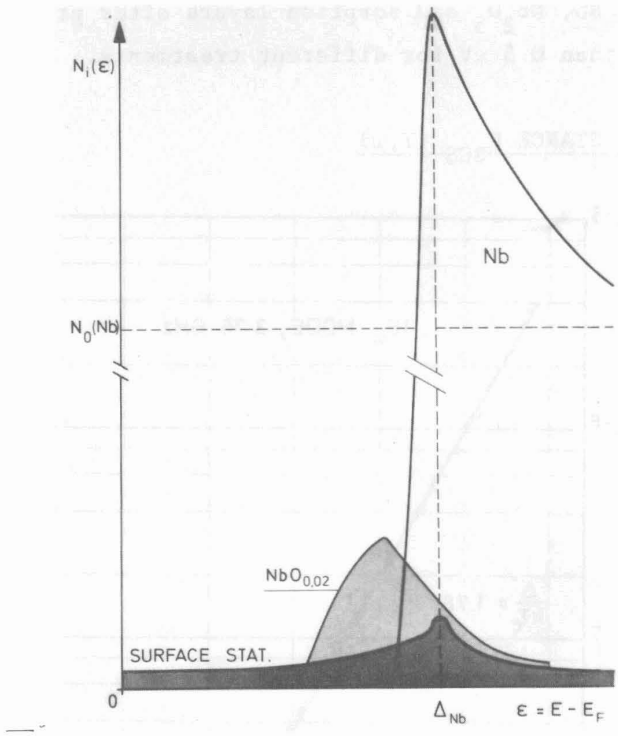

Fig. 2: Sketch of the density of bulk states $N(\varepsilon)$ and of surface states at oxidized superconducting Nb surfaces. Due to small (<< 50 nm) weak superconducting regions the BCS singularity is smeared out into the energy gap. If large (≈ 50 nm) suboxide (≈ $NbO_{0.02}$) regions exist states deeper inside the energy gap appear.

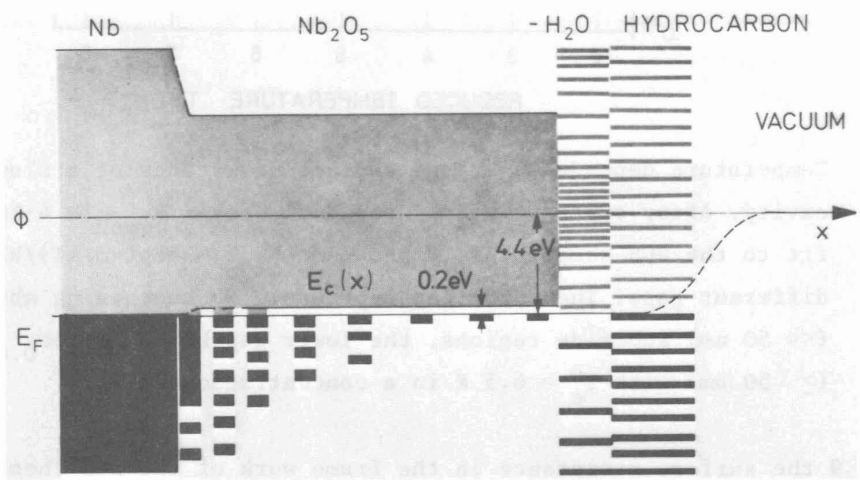

Fig. 3: Sketch of the electron states in Nb_2O_5 and its sorption layers. Due to the small ionization energy of oxygen vacancies of 0.2 eV, Nb_2O_5 is a semiconductor with appreciable conductivity at room temperature. The states in the sorption layers will not be arranged in bands because such layers are inhomogeneous.

The work function of Nb, Nb_2O_5 and sorption layers after prolonged pumping is not varying more than 0.5 eV for different treatments.

III. BCS SURFACE RESISTANCE $R_{BCS}(T,\omega)$

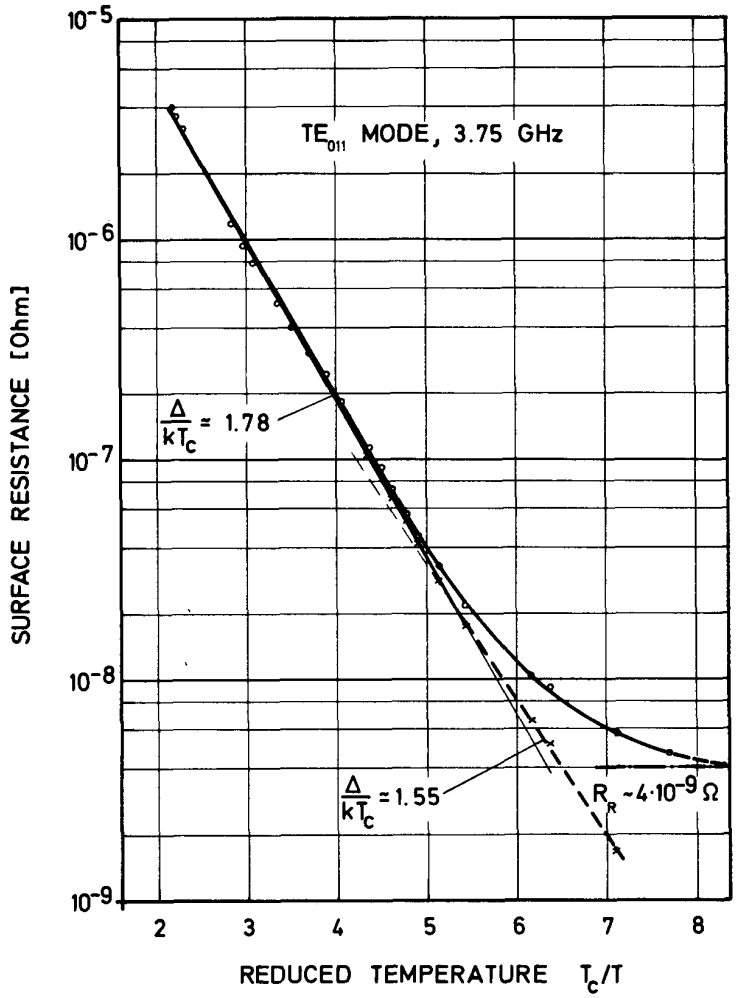

Fig. 4: Temperature dependence of the surface resistance of a slowly anodized cavity. After subtracting the residual losses $R_{resH} = 4 \cdot 10^{-9}$ Ω, the fit to the BCS temperature dependence $R_{BCS} \propto \exp(-\Delta/kT)/kT$ yields two different gaps. The upper gap represents Nb containing about 10% small (<< 50 nm) suboxide regions, the lower gap hints to $NbO_{0.02}$ lumps ($\gtrsim$ 50 nm) with $T_c^{**} \simeq 6.5$ K in a concentration of 2%. [4]

In Ref. 9 the surface resistance in the frame work of the BCS theory has been summarized assuming homogeneous and isotropic superconductors. As mentioned above Nb is not homogeneous and has states (Fig. 2) inside the energy gap of clean Nb, which has $\Delta(Nb) = 1.61$ meV corresponding to a $\Delta/kT_c = 2.02$. [6] These states "inside Δ(Nb)" lower the Δ/kTc-value deduced from the temperature dependence of

the surface resistance. For T > 2K, Δ/kT_c = 1.85 is typical, which seems to rise with frequency.[4] In addition, this fitted Δ/kT_c can depend on temperature, as shown in Fig. 4, if some low lying excitations (Fig. 2) exist. Such low lying excitations occur for weak superconducting regions being larger than the coherence length $\xi_{GL} \simeq 50$ nm. They can independently become superconducting - in our case for $\Delta^{\times}/kT_c^{\times} = 1.76$, $T_c^{\times} = 6.5$ K was obtained.[4] This result agrees with the $T_c^{\times} \approx 7$K obtained by penetration depth measurements shown in Fig. 5 for heat treated Nb. For heat treated cavities, R(T) did not show $\Delta/kT_c < 1.80$ indicating that the volume percentage of large regions with $T_c^{\times} \approx 7$ K is below 1%.

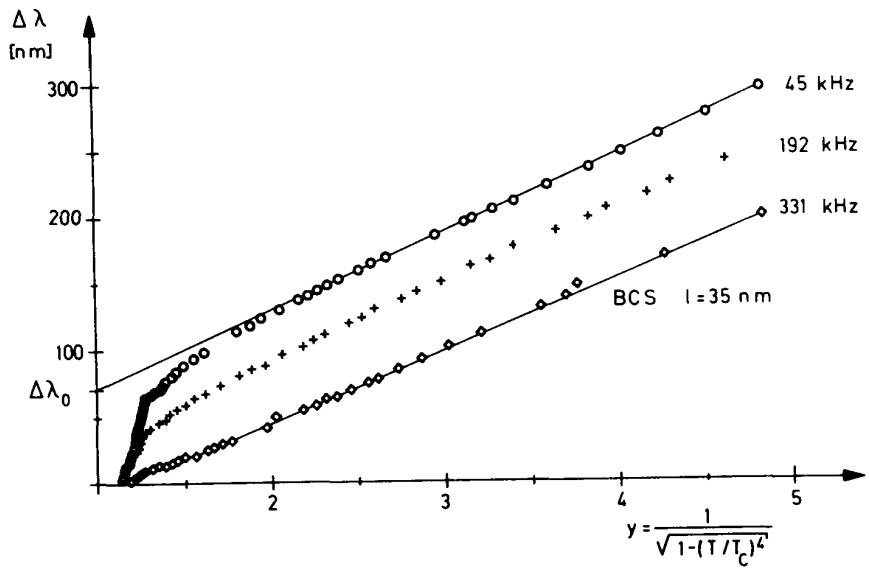

Fig. 5: Change of penetration depth versus $y = 1/\sqrt{1-(T/T_c)^4}$ for various frequencies at B_{ac} = 60 μT. The sample was fired at 1850°C for 2 h in a vacuum better than 10^{-10} mbar and handled in air for about 1 day. Fits to the data above 8.5 K yield a mean free path $\ell^{\times} \simeq 35$ nm and $T_c = 9.24$ K.[3]

Beside these effects of weak superconducting regions in Nb and of pair weakening at the Nb-Nb_2O_5-interface both depressing the Δ(Nb), the density of states gets smeared out [10] by these inhomogeneities as sketched in Fig. 2. This smearing reduces the surface resistance and yields $R_{BCS}(4.2K) \propto f^2$ below 5 GHz ($\hat{=}$ 0.016Δ(Nb)) as shown in Fig. 6. Between 12 and 18 GHz $R_{BCS}(4.2K) \propto f^{1.6}$ has been found (Fig. 6) which agrees with the BCS theory, indicating that the smearing of the BCS singularity is of the order of Δ(Nb)/50.

If the weak superconducting regions have sizes $d \gtrsim \xi_{GL} \approx 50$ nm, a magnetic field can drive them normal conducting at $T_c^{\times} \approx 7$K - see Fig. 5.[3] Such large regions seem to

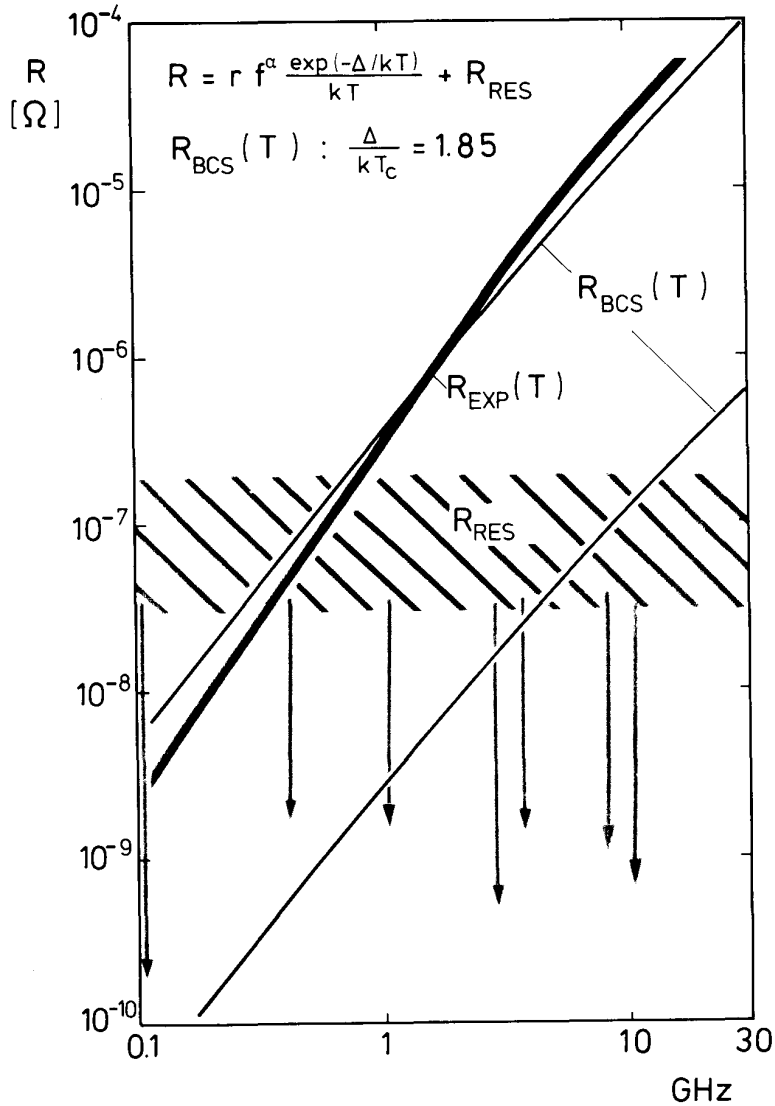

Fig. 6: Summary of experimental (▪) and computed (-) surface resistances of Nb between 0.1 and 30 GHz. The R(4.2 K,f)-values show the cross over of experimental and computed values due to the smearing of the BCS singularity. The differences of the computed slopes at 4.2 K and 1.8 K are due to the growth of $\hbar\omega$.
The residual losses show a large scatter depending on surface preparation. The arrows (↓) indicate best values.

occur in larger numbers and sizes [4] after anodizing or electron impact. [3] Such regions have a thermodynamic critical field $B_c^{**} \gtrsim 100$ mT, where at T = 0 the transition to the normal conducting state occurs. Below B_c, the BCS surface resistance depends on field only weakly. [11,12] So the field dependencies observed [13,14] are due to deviations from thermal equilibrium which will be discussed in Part. V. Because these deviations increase with increasing frequency, the above mentioned

frequency dependencies could be caused by deviations from thermal equibrium also.

IV. RF RESIDUAL LOSSES

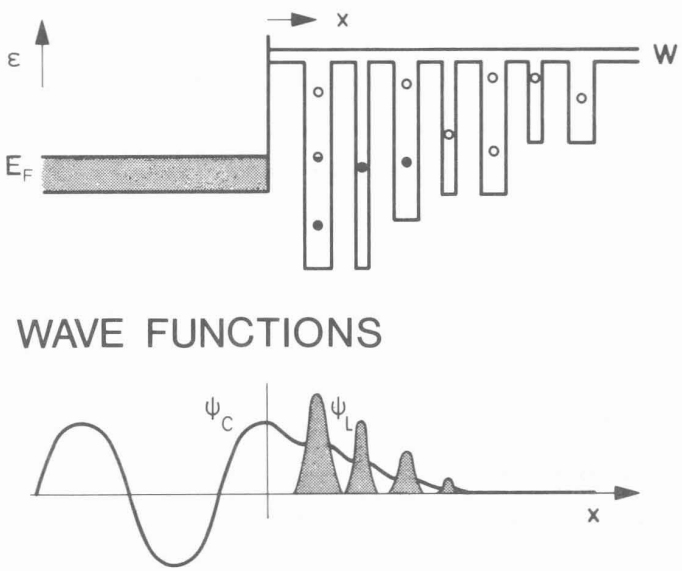

Fig. 7: Model metal-oxide interface showing the overlap of conduction electron (ϕ_c) and localized electron (ϕ_L) wave function, which corresponds to hybridization. The hybridization allows the transfer of perturbation from the system (ϕ_c) to (ϕ_L) or vice versa and enhances tunneling.

As shown in Fig. 4, with decreasing temperature the residual losses dominate, which are summarized in Fig. 6. As outlined in Refs. 15 and 16, these rf residual losses are due to interface states: As sketched in Fig. 7, conduction electron decay into the oxide like, $\exp(-\kappa x)$ and hybridize in the oxide with localized electron states n_L forming so new interface states, where properties of extended and localized states are mixed (Fig. 7). So momentum gained as extended state can be transfered to localized states exciting so phonons. The transfer is given by the beat frequency: [15,16]

$$\nu_E(x) = \frac{4}{h}\Gamma(x) = \frac{4}{h}\Gamma\ (0)\ \exp(-\kappa x)\quad \kappa = \sqrt{2m(E_c(x)-E_F)}\hbar^{-1} \qquad (1)$$

with $\Gamma(0.3\ \text{nm}) \simeq 1$ eV, and $\kappa^{-1} \simeq 0.5$ nm

So the rf shielding currents, given by $H_{\parallel}$, excite transverse phonons [15] proportional to $(\int \nu_E(x)\, n_L(x)dx)^2$: [15]

$$P_H = \frac{R_{resH}}{2} H_{\parallel}^2 \quad ; \qquad 10^{-7} > R_{resH}(\text{GHz}/f)^2/\Omega > 10^{-12} \qquad (2)$$

The longitudinal electric rf field $E_\perp(t)$ excites longitudinal phonons:

$$P_H = \frac{\varepsilon_0}{2\mu_0} R_{resE} E_\perp^2 \quad ; \qquad R_{resE} \lesssim 10^{-4}\ \Omega/\varepsilon_r^2 \qquad (3)$$

Both residual loss mechanisms sensitively depend on the hybridization and so on the conduction band in the oxide via κ (Eq.(1)) and on the density of localized states n_L near the Fermi energy. So, the residual losses are changed by surface treatments or rf processing. But it should be mentioned that chemical residues from cleaning or dust cause locally enhanced (electric) residual losses dominating at low frequencies - see Eq. (3) or Fig. 6.

V. DEVIATIONS FROM THERMAL EQUILIBRIUM

In the frame work of the BCS theory, the surface impedance increase only by 20% [11,12] up to the critical superheating field B_{sh} ($\simeq B_c$(Nb)), whereas experimentally much stronger field dependencies have been observed: At fields as low as $B_c/100$, R decreases with B_{rf} [13], as shown in Fig. 8, or R increases markedly with B_{rf} - see Fig. 9 - showing an rf breakdown around $B_c/10$. All these effects can be related to deviations from thermal equilibrium, which are not included in the BCS treatment.

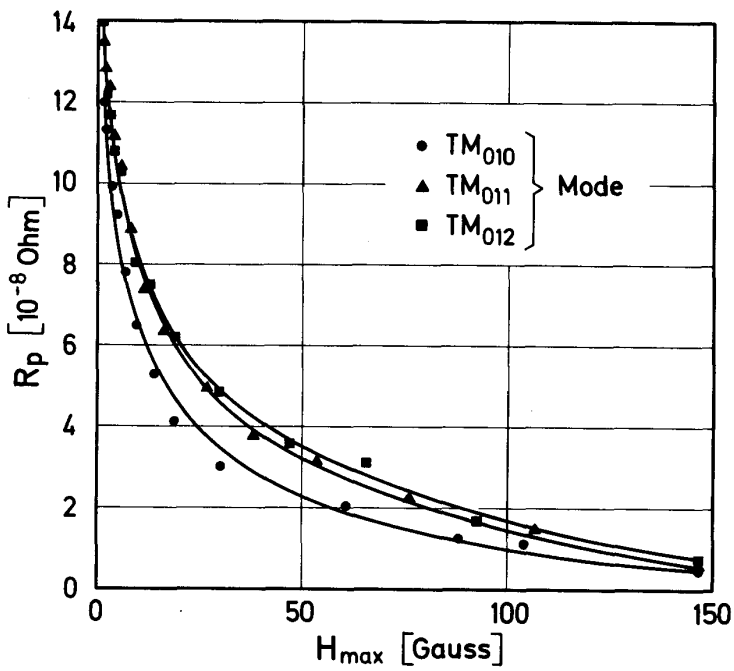

Fig. 8: Component of the surface resistance which depends strongly on rf field level [13] for the mode family TM_{01n} (n=0:2.17GHz; n=1:2.61GHz; n=2:3.62GHz) at 1.2K. The analysis of the experimental curves results in $R_p \propto \omega^{\alpha(H)}$ with $0 < \alpha(H) \lesssim 0.6$.

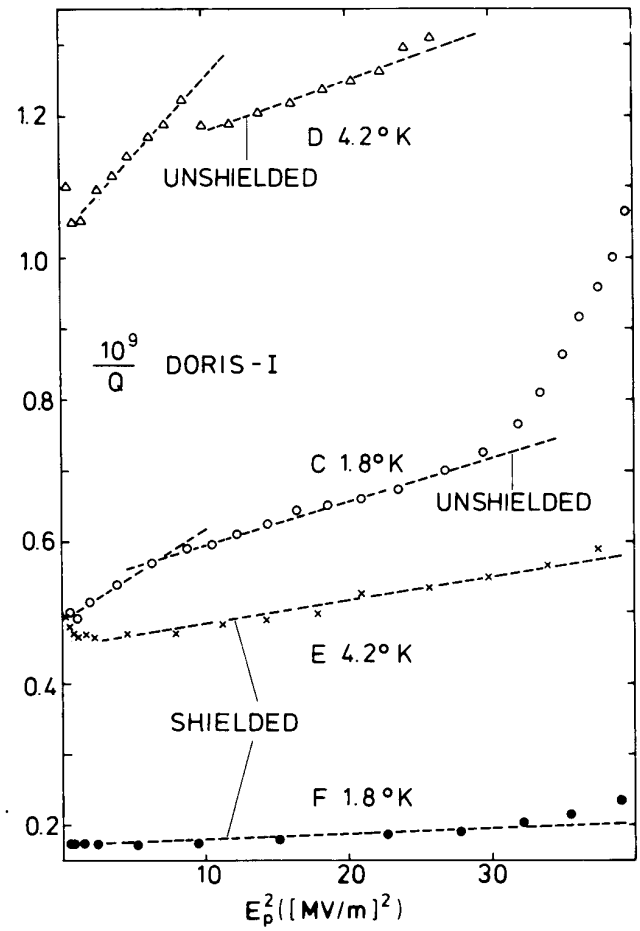

Fig. 9: 1/Q plotted versus E_p^2. The straight lines above 3 MV/m, with slopes $\gamma \simeq 50$, reflect the growth of normal conducting regions detected also by heat pulses. [14] The kinks around 3 MV/m are likely due to a change in cooling. Because above 3 MV/m γ does not change with temperature and Q_o, the cooling in He is the same at 1.8 and 4.2 K.

The first effect - Fig. 8 - is due to the long inelastic relaxation time of electrons with phonons τ_{in}: [17]

$$\tau_{in}(Nb) = 1.5 \cdot 10^{-10} (T_c/T)^3 \text{ sec}; \quad \ell_{in} = 10^{-2}(T_c/T)^3 \text{ cm} \qquad (4)$$

i.e. the quasiparticle system is decoupled from the phonons the more the lower the temperature is. But also the phonons are not in thermal equilibrium as shown by their long relaxation time or mean free paths. E.g. at 4 K one can obtain [17]

$$\ell_{ph} \simeq 2.6 \text{ cm} \qquad (5)$$

So deviations from thermal equilibrium will play a major role in superconducting Nb cavities. In the following two types of deviations will be discussed: Deviation of the quasiparticles alone from thermal equilibrium and deviation of the quasiparticle and phonon temperature from the temperature of the He bath.

In the penetration region quasiparticles absorb rf photons in a rate [17] τ_{ab}^{-1} (1 mT) $\simeq 10^{+9}$ sec^{-1}, which because of $\tau_{ab}^{-1} \propto H^2$, soon yields <u>deviation from the thermal equilibrium</u> because of $\tau_{ab} \ll \tau_{in}$. For homogeneous superconductors this bottleneck is no problem, because the quasiparticles excited in the penetration region can transfer their energy in the bulk to the phonons. In contrast, states localized in the penetration region cannot escape into the bulk and so the bottleneck will build up, finally yielding a constant distribution function for states below Δ(Nb). So the rf absorption from regions with depressed Δ will diminish with H as found for weak superconducting regions - see Fig. 8 and Ref. 13 - and for normal conducting regions - see Ref. 3. Only in cases where the quasiparticles are strongly coupled to phonons as in "amorphous superconductors" (ℓ < 5 nm) or in normal conducting regions extended far into the bulk, equilibrium R(T)-values can be used.

The <u>quasiparticle and phonon temperature T^* can be enhanced over T_{He} of the He bath,</u> but because of the large ℓ-values (Eqs. (4) and (5)), T^* cannot be evaluated by the usual heat conductivity equation: [18]

$$\Delta T = T^* - T_{He} = \frac{R}{2} H^2 \sum_i \frac{d_i}{\kappa_i} \qquad (6)$$

where d_i/κ_i are the different heat resistances. It should be mentioned that especially for normal spots ($R_{nc} H^2/2$) lateral heat flow in the Nb and the addition of heat flows $(R_{nc}+\alpha R_{sc})H^2/2$ from different sources asks for a 3 dimensional treatment. The temperature increase ΔT increases the surface resistance R(T) which can be described by: [19]

$$\frac{\Delta R}{R_o} = \frac{\Delta T}{R_o} \frac{\partial R}{\partial T}\Big|_{T^*} = \frac{R H^2}{2 R_o} \sum_i \frac{d_i}{\kappa_i} \frac{\partial R}{\partial T}\Big|_{T^*} = \gamma \left(\frac{H}{H_c}\right)^2 \qquad (7)$$

For cases where $R \simeq R_o$ holds, γ will be independent of R_o and nearly temperature independent below 0.8 T_c because the dominating electronic heat conductivity κ has the same temperature dependence as R. For $T^* \lesssim 5$ K, $\gamma \lesssim 1$ can be evaluated and such small increases have not been observed, yet.

As shown in Fig. 9, γ's $\gtrsim 50$ have been observed and such strong increases are due to the growth of normal conducting regions A_{nc}: [19]

$$\frac{\Delta R}{R_o} = \frac{R_{nc}\,\Delta A_{nc}}{R_o A_{sc}} = \gamma \left(\frac{H}{H_c}\right)^2 ; \quad \Delta A_{nc} = \Delta T \; C_{nc} \qquad (8)$$

Without numerical calculations the growth rate C_{nc} cannot be estimated. Experimental results [14] - Fig. 9 - show that also in this case γ is nearly independent of R_o changing with T or frozen in flux, indicating that the effective $\Delta A_{nc} \propto \Delta T \propto (R_{nc} + \alpha R_{sc})H^2$ is dominated by $\alpha R_{sc} > R_{nc}$. This indicates, that the growth is not given by the normal conducting regions but by superconducting regions with their losses, which are rapidely rising with temperature. This astonishing experimental result is well known from normal conducting regions in flux cores. [20]

VI. RF BREAKDOWN

As outlined in Ref. 21, the rf breakdown is due to a thermal explosion driven [18] by the more than 10^4 times larger rf losses in normal conducting regions as compared to the superconducting state. The beginning of this explosion at B_{crit} can be due to the occurence of normal conducting spots at their local critical superheating field B_{sh} or due to a instability of the heat conductivity equation. [18] But small normal conducting regions embedded in superconductors have by more than 2 orders of magnitude reduced normal conducting losses [3] due to deviations from thermal equilibrium. [17] And, as shown also above, large normal conducting regions stationarily exist in superconductors as fluxoids [20] or as larger regions, which grow like H^2 with field. For small normal conducting regions (< 0.5 cm^2) the rf breakdown seems not to be caused by normal conducting losses but mainly by superconducting losses and by impinging electrons. [14]

So, beside some qualitative theories [14,18,21] there exists no quantitative theory for the rf breakdown.

VII. ELECTRON EMISSION OUT OF EXCITED STATES

Electron loading in superconducting rf cavities is classified in multipactor (MP) and field emission (FEM) loading [22] as outlined in Part. VIII. Experimentally, both types of loading are very sensitive to the sorption layers and in both cases, electrons hit the emitting surface. [22] So, first the excitation, relaxation and emission of such states will be discussed. Secondly this will be applied to secondary emission of Nb-Nb_2O_5 ... surfaces. And thirdly the rf FEM of such surfaces will be discussed.

1. Excitation, relaxation and emission of electrons

Electrons impinging solids are slowed down by exciting electron hole pairs of energy around 30 eV. [2,23-25] These excited states of density $n_e(\vec{r},E)$ relax by electron-electron (plasmon) interaction τ_{e-e}^{-1}, by phonon (LO) interaction τ_{LO}^{-1}, [26] by escape into the vacuum τ_v^{-1} and by field emission τ_{FEM}^{-1}. τ_{e-e}^{-1} and τ_{LO}^{-1} are proportional to mean free pathes ℓ_{e-e} and ℓ_{LO}. All these relaxation and emission rates depend on position $\vec{r}$ and on excitation energy E, and so the (transport) equations for $n_e(\vec{r},E)$ are very complicated. In Ref. 23, the transport equation using τ_{e-e} and τ_{LO} has been used to treat secondary electron emission. A simplified version of this approach reads as follows: [2,25] Neglecting band structure effects and electron diffusion, the electron-electron interaction soon ($\simeq 10^{-14}$sec) [26] thermalizes the electrons to a distribution function:

$$\frac{dn_e}{dE} = \frac{n_e}{\bar{E}} e^{-\frac{E}{\bar{E}}} \qquad (10)$$

with $\bar{E}(=k\bar{T})$ as mean energy ($\simeq$ 8 eV) [25] and n_e the overall concentration of excited states being proportional to, e.g., the impinging electrons. This cloud of excited electrons relaxes ($\simeq 10^{11}$ eV/sec) [26] by phonon emission and is scattered by electrons and phonons [26] in approaching the surface. Hitting the surface barrier, electrons with an energy E smaller than the electron affinity χ, will be reflected totally and for $E > \chi$ partially with a reflection coefficient R(E):

$$R(E) \simeq 1-4\sqrt{\frac{E-(\chi+E_F)}{\chi+E_F}} \qquad (E-\chi>>\chi) \qquad (11)$$

For semiconductors E_F has to be substituted by zero because E and χ are then relative to the conduction band edge. So with Eq. (10) as inner distribution of excited electrons, one gets as outer distribution:

$$n_t(E) = \frac{1}{2} n_o\left(1-\frac{\chi}{E}\right) \exp\left(-\frac{E}{\bar{E}}\right) \cdot R(E) \qquad (12)$$

which is well known as distribution of the true secondary electrons - see SE in Fig. 10. The factor $(1-\chi/E)$ in Eq. (12) is due to the finite mean free path ℓ. [25] The true secondary electrons escaping per incident electron are given by: [25]

$$\delta_t \propto \int_{\chi}^{\infty} dE \frac{\lambda_a n_t(E)}{2} \simeq \lambda_a \exp\left(-\frac{\chi}{\bar{E}}\right) \qquad (13)$$

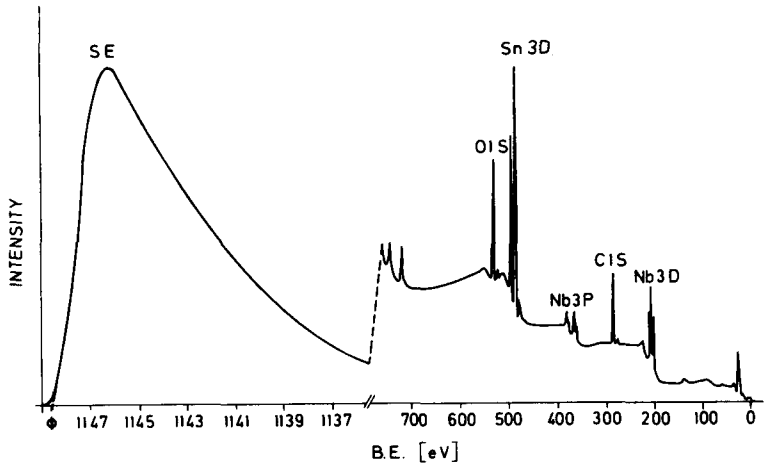

Fig. 10: XPS spectrum [1,2] of a Nb_3Sn surface coated by oxide and sorption layers. The labeled peaks are used for the studies of Nb, Nb and Sn oxides, O in oxides, adsorbed C and O and secondary electrons SE, where the latter contain about 80% of all photoelectrons. The secondary electron distribution curve (EDC) shown, is typical for the true secondaries δ_t, i.e. excited states distributed like $\exp(-E/\bar{E})$ emitted across a barrier of height $\chi \simeq \phi$. This work function ϕ is defined by the intercept of the steepest slope with the axis. [2]

In metals and semiconductors $\lambda_a = \ell_{e-e}$ is short and so the secondary yield is about $\delta_{tm} \simeq 1.5$ at maximum. In insulators the electron electron scattering is missing and hence $\lambda_a (> \ell_{LO})$ is large and $\delta_{tm} \simeq 10$ has been found. [24] Also the distribution $n_t(E)$ depends on the dominating type of relaxation: For emission out of a conduction band with dominating ℓ_{e-e} scattering, $n_t(E)$ has a maximum around $E-\chi \simeq 2$eV, whereas for insulators the maximum is around 1 eV. [24] For localized surface states the maximum can be even closer to χ because then also R(E) is enhanced like in resonance tunneling.

For rf cavities also the time between impact and emission has to be discussed. The mean energy of secondary electrons is about $\overline{E-\chi} \approx 1$eV, which corresponds to a frequency [15] $\nu_E \simeq 10^{15}$ Hz. So for GHz cavities the secondary electrons are emitted instantaneously.

If an electric field is applied to such a surface, the excited states will be emitted the stronger the higher their excitation energy is like in the case of F-T [28] and photo field emission [29]. Because states having energies well above χ relax or are emitted fast in an rf field, states with $E \lesssim \chi$ will be emptied by an applied electric field E. As sketched in Fig. 11, the density of such states is

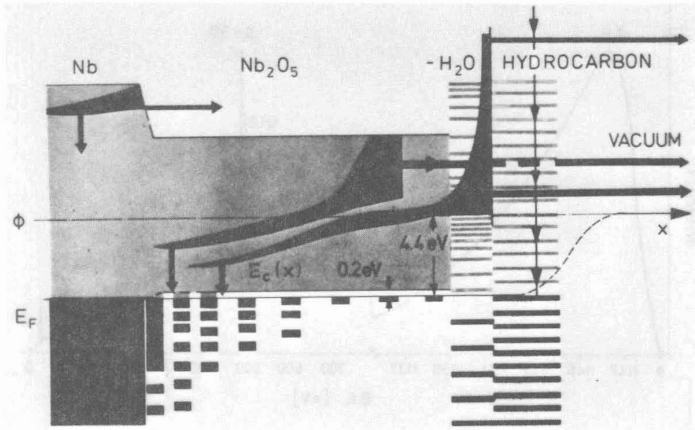

Fig. 11: Sketch of excited states in Nb-Nb_2O_5 sorption layers. The fast electron-electron interaction in Nb and Nb_2O_5 thermalizes the states to $n_e \propto \exp(-E/\bar{E})$ with $\bar{E} \approx 8$eV. The slow emission of longitudinal optical (LO) phonons (↓) relaxes the excited states if no emission (→) into the vacuum occurs. Localized states in the sorption layer approach equilibrium by emission into the vacuum and the slow LO emission. Conditioned - polymerized - hydrocarbons show enhanced absorption and relaxation of slow electrons.

very high and so the emission will be very strong- see Fig. 12 - and proportional to the impinging electrons. The emission time [22] will be quite short in this case because of the low and narrow tunnel barrier.

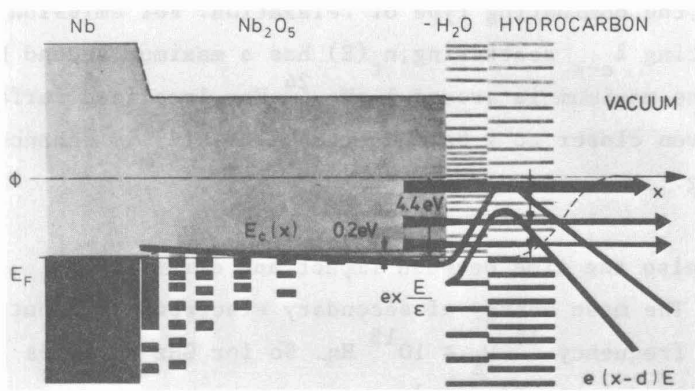

Fig. 12: Sketch of the field emission of a Nb-Nb_2O_5 .. surfaces with excited states. Because ,according to Fig. 11,the density of such states at Φ is very high their emission dominates the electron current. The barrier is very small for states in the sorption layer and so, e.g., Nb_2O_5-H_2O enhances the field emission very much by resonance tunneling. Polymerized hydrocarbons can absorb slow electrons and will so reduce the field emission current, especially because this absorption enhances the work function.

2. Secondary electron emission from Nb-Nb_2O_5 ... surfaces

To analyze the secondary yield of the Nb sketched in Fig. 1 we start with the yield of Nb and Nb_2O_5. The maximum in the true yield occurs at about 300 eV with $\delta_{tm} \simeq 0.8$. [2] For clean Nb_2O_5 the true yield is about $\delta_{tm} \simeq 1.1$ and not depending on temperature, [30] despite the fact that Nb_2O_5, as semiconductor with 0.2 eV activation energy (Figs. 11 and 12) becomes an insulator at He temperature. But according to electron current [14,31] or yield measurements [2,30] typical electron currents are above 10^{-9} A/cm^2. Because the secondaries are a small percentage of the excited states of a surface layer $\lambda_a \simeq$ 5nm, the density of excited electrons is well above 10^{19}/cm^3.

Then according to Ref. 26, the fast electron-electron scattering dominates yielding, e.g., $\lambda_a \simeq 5$ nm. [1,2] For such impinging electron currents (>> nA/cm^2) λ_a is short and temperature independent. The higher yield of Nb_2O_5 as compared to Nb could be due to the smaller electron affinity of Nb_2O_5 (0.2eV) - see Eq. (13), which also reduces the reflection coefficient R (Eq. (11)). The latter effect of enhancing the yield by reducing the reflection at $E \gtrsim \chi$ is fairly effective because the density n_e (Fig. 11) is very high at $E \gtrsim \chi$. The reflection coefficient is reduced further, by the Nb_2O_5-H_2O chemisorption state, because the peak in $n_t(E)$ occurs well below $E-\chi = 1$ eV - Fig. 13 - and

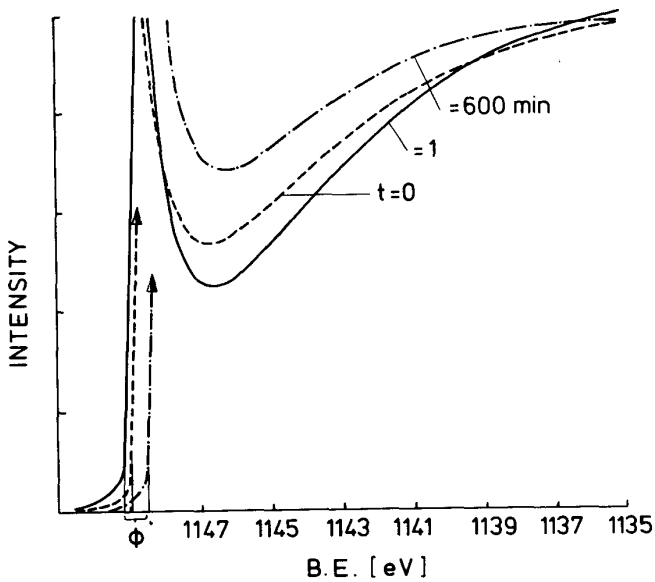

Fig. 13: EDC's of secondary electrons emitted by excited states of wet Nb_2O_5. [1] The two peaks indicate the existence of electron emitting levels of the Nb_2O_5-H_2O chemisorption state below ϕ and around ϕ+10eV. The electrons being emitted out of the Nb_2O_5 conduction band (Fig. 11) seem to be resonantly scattered into the Nb_2O_5-H_2O states. With enforced polymerization of the hydrocarbons by electron impact, more - slow - secondary electrons get absorbed by the hydrocarbons lowering the yield δ_t (Fig. 14).

the yield δ_{tm} is enhanced up to 2. Because in this case the true peak of Nb_2O_5 at χ + 2eV cannot be seen, the Nb_2O_5-H_2O seems to form a dense layer and the excited electrons of Nb_2O_5 are resonantly scattered into states around χ and χ+10eV from where they are easily emitted because of the small R(E).

An other way sorption layers on Nb_2O_5 enhance the yield is by the reduction of the surface barrier $\phi \simeq \chi$.[2] But according to Eq. (13) and Fig. 14, ϕ changes by less than 0.6 eV, which is insufficient to explain the about 50% yield reduction observed (Fig. 14)[2]. As outlined in Ref. 2, the yield reduction is due processes absorbing electrons in the insulating sorption layers by which negative charging occurs measured by C peak shifts or as ϕ increase.[2] I.e. charging in insulators indicates enhanced (or reduced) electron absorption. If thick enough H_2O sorption

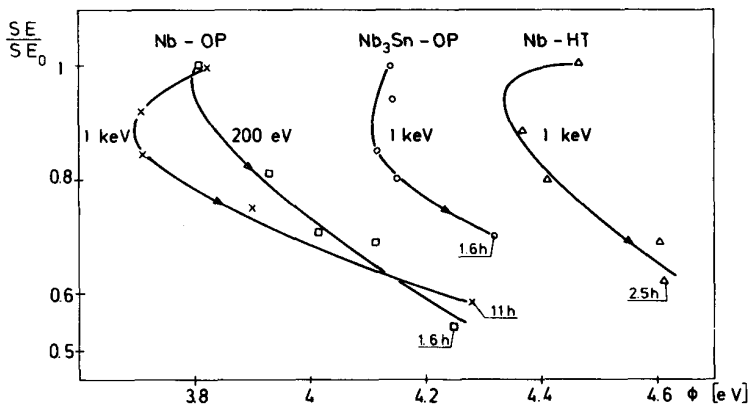

Fig. 14: Yield changes[2] $SE/SE_o = \delta_t/\delta_{to}$ versus work function of 3 Nb samples (OP: oxipolished; HT = annealed in UHV at 1850°C for 2 h)[1] and one Nb_3Sn sample, subject to electron impact (100 $\mu A/cm^2$). The final duration of the electron impact of 1.1 - 11 h corresponds to electron doses between 0.4 and 4 Coulomb/cm^2.

layers ($\lesssim$ 1.5 nm) exist, which lower ϕ by 1 to 2 eV as inferred from asymmetric tunnel characteristics,[8] the yield can be drastically enhanced. This layer seems to be evaporated by prolonged pumping in UHV and so it was not found in the XPS and secondary yield measurements.[2,30]

Above it was mentioned that the sorption layers are insulating and then the long λ_a(> 20 nm) should enhance the yield. But because the sorption layers - after prolonged pumping - see Ref. 2 - are only about 3 nm thick, this mechanism enhances the yield not more than 10%.

The most dramatic effect in the secondary emission of Nb is the reduction of the yields δ_t by about 40% by electron impact of 1 C/cm^2 - see Fig. 14. As discussed in Ref. 2, this yield decrease seems to be due to an electron impact induced polymerization involving hydrocarbons. This polymerization yields low lying ($\sim\phi$) electron states which resonantly absorb electrons and which relax fast. Details of this polymerization are not known, but the effect is dramatic, stable at He temperature but not stable at room temperature.

3. Rf field emission of Nb surfaces sketched in Fig. 1

Nb with its oxide and sorption layers has a work function above about 4 eV as summarized in Fig. 14. So the field emission current will be negligible [28] up to fields of $2\cdot10^9$ V/m. Because electropolished Nb has nearly no roughness, a field enhancement factor $\beta_G \simeq 100$ is an upper limit and so below $(2\cdot10^9 \text{V/m})/100 = 2\cdot10^7$ V/m no field emission current should be observable. Thus, the observed FEM loading at [14,31] 5 MV/m can only be due to FEM from excited states - see Fig. 12. Thermally excited states, e.g. due to heating proportional to E_p^2, would yield an upward bending of the Fowler-Nordheim plot - see Fig. 4 in Ref. 28 - which has never been observed - see, e.g. Fig. 15. In contrast, in some cases a downward bending has been observed. So, one has to explain the Fowler-Nordheim dependence shown in Fig. 15 by other excited states. As discussed above - see Fig. 12 - electron impact excites states, which around ϕ are easily drawn by an electric field out of the dielectric sorption layers ($\lesssim\lambda_a$) where they in addition can gain the energy $\lambda_a\, eE/\varepsilon_r$.

As indicated in Fig. 11 the density of excited states around ϕ is very high and their relaxation is fairly slow and given by $\exp(-t/\tau_o)$ with $\tau_o \approx 10^{-10}$ sec. [26] Neglecting mirror charge effects the FEM out of excited states of energy E is given by ($E_c = E_F$):

$$j_{FEM} \simeq e^{-\frac{4}{3}\kappa\frac{\phi-E}{E_p}} = e^{-\frac{c}{\beta E_p}} ; \quad \kappa = \sqrt{2m(\phi-E)}/\hbar \qquad (14)$$

Comparing this current with one assuming $\phi-E \simeq \phi = 4$ eV one obtains as correction factor in the exponent

$$\frac{1}{\beta^*} = \sqrt{\frac{\phi-E}{\phi}}\,\frac{\phi-E}{\phi} \qquad (15)$$

yielding for $\phi-E = 0.4$ eV $\beta^* = 31$. So β-values of 10^3 fitted to experimental data [14,31-34] hint to emission out of states excited to about $\phi-0.4$ eV. This type of FEM is proportional to the electron impact and varies slowly with ϕ like $\exp(-\phi/\bar{E})$

- see Eq. (13). So β changes observed hint to changes in $\overline{\phi\text{-}E}$, i.e. to changes in the states in the sorption layer. Chemisorption states and other states in front of Nb_2O_5 with its high $\varepsilon_r \approx 36$, will enhance the FEM in the sense of resonance tunneling.[27,34]

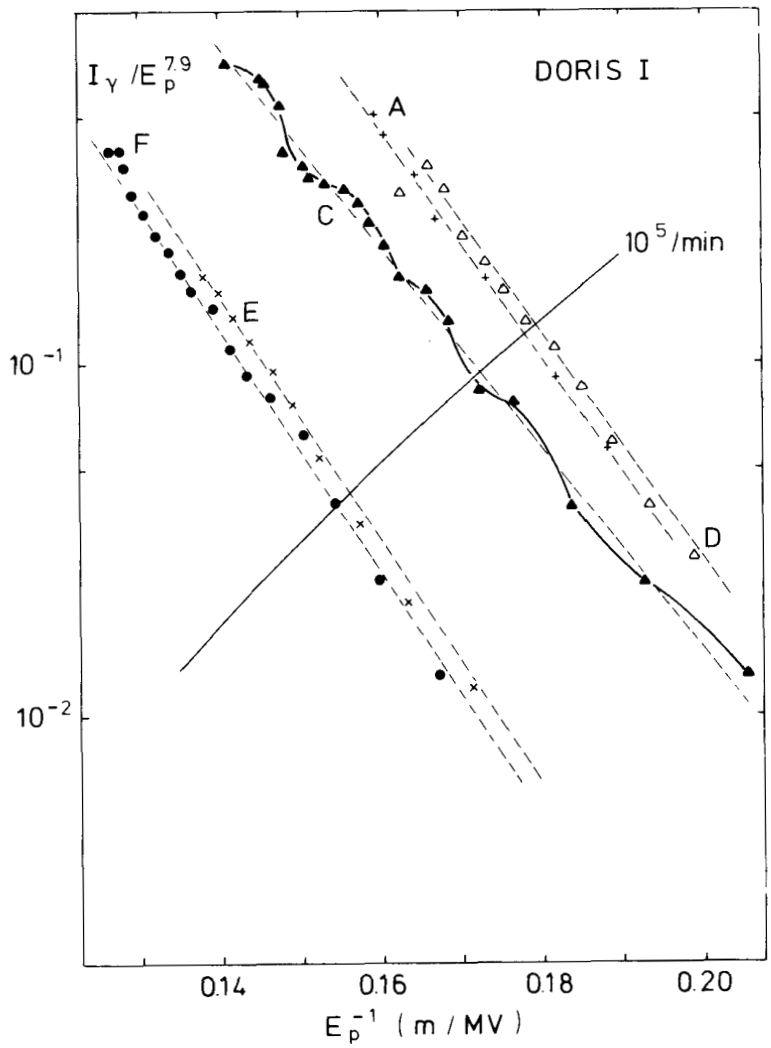

Fig. 15: Fowler Nordheim plot of the x-ray yield measured at the midplane of the cylinder of a 500 MHz TM_{010} mode cavity.[14] With impinging FEM electrons (rf conditioning) the FEM is reduced. This reduction is mainly due to a reduction of the emitting area, whereas the β(≈700)only decreasesby about 20%. The oscillations, which are most pronounced for run C, are an indication for emission out of excited states, which fits to the large β values.

Another hint to emission out of excited states is the oscillation on top of the Fowler-Nordheim dependence shown, e.g., run C in Fig. 15, which seems typical for tunneling through a thin barrier.[29] As already mentioned above, Nb_2O_5-H_2O

chemisorpion states inside the FEM barrier most likely channel excited states into the vacuum and so the oscillation in $j_{FEM}(E_p)$ could be due to E_p-field induced level splitting.

For the secondary emission the changes due to Nb_2O_5 and sorption layers have been discussed above and in Ref. 2. For FEM these changes with sorption layers can be even stronger because states in the FEM barrier can enhance the FEM much stronger than the secondary emission, but less quantitative information is available in the case of FEM. The above summarized ideas offer some qualitative explanations for the FEM changes observed with surface treatment, rf processing or He-conditioning (Refs. 14, 22, 31-34):

- $\beta \approx 10^3$ hints to emission out of states with $\overline{\phi-E} \lesssim 0.4$ eV, which could be the states of Nb_2O_5-H_2O found by the EDC (Fig.13) slightly below ϕ.
- β changes with He-conditioning [34] can be explained by an increase of $\overline{\phi-E}$ e.g., due to sputtering off the H_2O or by positive charging of the sorption layers.
- The reduction of j_{FEM} by rf conditioning seems to be due the enhanced absorption of slow electrons by polymerized hydrocarbons. So mainly the emitting area is reduced and not β - in agreement with some experiments - see, e.g., Fig. 15. [14] But if this absorption charges the sorption layer negatively the enhanced ϕ should reduce β. [14]

The following points, which are important for the analysis of experimental results, should be mentioned:

As outlined in Ref. 22, FEM decreases with increasing frequency because of the finite beat frequency. This beat frequency increases exponentially with E_p reducing the fit parameter β up to a factor 1/3. [22] Because in rf cavities FEM out of excited states will occur also at $E_p(t) = E_p \cos\omega t < E_p$, the fitted β is enhanced also by this effect. So, e.g., the downward bending of the Fowler Nordheim plot could also be due to shift of the FEM to earlier phases.

VIII. ELECTRON LOADING IN SUPERCONDUCTING Nb CAVITIES

In Part VII the mechanisms important for emitting electrons from Nb covered by Nb_2O_5 and sorption layers have been discussed. Whereas the secondary emission is now fairly well understood, [2] the mechanisms governing rf field emission are just becoming clear. But because both processes are intermingled in rf cavities, first the evolution of the electron emission will be discussed, and then the type of loading encountered.

1. Electron currents in an rf cavity

Assuming some impinging electrons, e.g., from noise, onto a surface with $E_\perp = E_p \cos\omega t$ present, the fast electrons escaping during the time $-\pi/2 < \omega t < \pi/2$ will be slowed down by $E_\perp$ and so they loose energy and most are accelerated back to the surface. Only fast, i.e. backscattered, electrons can escape. Because true secondaries have energies below 5 eV and because their secondary yield is about 1, the secondaries emitted in $\{-\pi/2, \pi/2\}$ are collected at the surface. At $\omega t \gtrsim \pi/2$ these electrons are accelerated away from the surface. Electrons impinging at $\pi/2 < \omega t < 3\pi/2$ produce instantaneous secondaries and excited states, E_p will draw electrons out of the excited states proportional to $\exp(-c/E_p(t))$ and this FEM will decay like $\exp(-t/\tau_o)$ with $\tau_0 \gtrsim 10^{-10}$ sec - see Part. VII. The amount of electrons impinging at the different phases depends on the trajectories, which will be discussed in Part. VIII.3. Here it should be mentioned only, that electrons with impact energies between 100 and 2000 eV are most effective in producing secondaries and excited states.

2. Multipactor loading (MP)

As discussed, e.g. in Refs. 22 and 32, multipacting occurs at well defined field levels with starting phases $\omega t \gtrsim \pi/2$. So secondaries produced during the wrong E_p direction ($< \pi/2$) are stored and will be accelerated into MP phase regions, i.e. they will enforce MP. Because electrons gain energy on MP trajectories, the "background loading" will be enforced in these field regions. For example, the second order one side MP shows up in a peak on the background FEM current as shown in Fig. 4 of Ref. 31.

Another example is two side MP: At such levels the electrons stored during $\omega t < \pi/2$, the secondary electrons and the field emitted electrons out of excited states will enhance the MP levels - see, e.g., Ref. 14 for orders $n \approx 20$ and Ref. 31 for $n = 1$ ($d_{gap} = 11$ cm). Due to the high E_p-field, FEM is the dominating enhancement mechanism in the latter example.

This discussion shows, that dc secondary yields can be enhanced very much in rf cavities due to the storage of slow electrons and due to FEM out of excited states which explains the occurence of MP levels, where the dc yield is still smaller 1. Because the FEM out of excited states is changing more strongly than the secondary yield with variations of the sorption layers, this effect can explain the success of rf or He conditioning in overcoming MP levels. [14]

3. RF field emission loading

The rf FEM loading seems the ultimate limitation in superconduting Nb cavities, yielding for narrow gap ($d_g < \lambda/2\pi$) cavities about $E_p \approx 20$ MV/m [22,31,32] and for wide gaps ($d_g > c/\omega = \lambda/2\pi$) about $E_p \simeq f16$ MV/m GHz. [31,32] The appearance of the FEM loading is an electron current $j_{FEM} \propto \exp(-c/\beta E_p)$ (Eqs. (14) and (15)) with $100 \lesssim \beta \lesssim 2000$, [22,32] which is shape and frequency dependent and which initiates rf breakdown by heating [14] or limits the attainable fields simply by the absorbed rf power. [31-34]

As already mentioned above, the high β-values together with the oscillations - see Fig. 15 - hint to FEM out of excited states-especially states in the FEM tunnel barrier - which explains its sensitivity to surface treatments like rf or He conditioning.

The question to be discussed in this part is then: where are the excitations coming from and why is this depending on shape and frequency?

The observations that FEM loading in narrow gap cavities ($d_g < \lambda/2\pi$) limits E_p to about 20 MV/m and that β-values are often smaller than in wide gap cavities, can be explained as follows: Electrons emitted around $\omega t \simeq \pi$, where E_p is maximal, hit the opposing surface shortly afterwards. There, at this time E_p is still slowing down emitted electrons and so nearly all excited states will disappear like $\exp(-t/\tau_o)$. So the "temperature" of the excited states (around ϕ) in the sorption layer will be fairly low yielding $\beta \simeq 200$. [31]

In contrast in wide gap cavities, electrons emitted around $\omega t = \pi$ will return roughly 2π later to the emission region with small impact energies. So electrons are excited at $\omega t \simeq 3\pi$ where the large E_p-field enlarges the secondary emission by FEM out of excited states. In parallel plate geometry the maximum excursion distance d_{max} is given by: [35]

$$d_{max} = \frac{\lambda}{2\pi} \operatorname{arctg} \frac{\lambda e E_p}{2\pi m_o c^2} \qquad (16)$$

That is for $\lambda e E_p/2\pi < m_o c^2$, $d_{max} \propto E_p$ grows with field amplitude, whereas for relativistic energies $\lambda e E_p/2\pi > m_o c^2$ the excursion no longer depends strongly on E_p, where

$$E_p = m_o c^2 (2\pi/\lambda e) = 10 \text{ MV/m GHz} \qquad (17)$$

holds.

In accelerator cavities E_p decreases due to beam holes and roundings with distance from the surface. So an electron starting at $\omega t = \pi$ will return in $\{2\pi + \alpha\}$. For the nonrelativistic case, where d_{max} increases with E_p, the trajectories see with increasing E_p more inhomogeneous fields, which lowers the return efficiency. For the relativistic case, d_{max} (Eq. (16)) becomes independent of $E_p \gtrsim 10 \cdot f$ MV/m GHz, i.e. independent of E_p some trajectories will return to the region where they have been emitted. At this spot, the electrons in the oxide and sorption layers get excited allowing so secondary and FEM emission with large β values. Because in this field region, the impact energy [35] ε scales like $\varepsilon \propto f^{-2}$, the number of excited states will diminish like f^{-2}. Thus β will decrease with increasing frequencies in agreement with experiments [22,32] if the large variations of β with sorption layers are taken into account. This is also an explanation why for f > 2GHz higher E_p fields have been obtained than for narrow gap structures.

The frequency dependence of the maximal field in wide gap cavities is with $E_{pmax} \simeq 16$ MV/m GHz in good agreement with Eq. (17) where this type of rf FEM loading should become dominant. According to the ideas outlined above, a strong decrease of E_p with distance from the surface for the high field region should weaken the loading, which would explain the differences between Refs. 31, 14 and 33 as due to larger beam holes and rounding. It is obvious that the above arguments can be made more quantitative only by trajectory calculations, [14,22,31,32] These have already shown that backscattered electrons will dominate the loading via their high yield δ (Nb) = 0.42.

An elliptically shaped cavity should - besides theoretical and cleaning arguements - show reduced FEM loading [36]

References

1 M. Grundner, J. Halbritter, J. Appl. Phys. 51, 397 (1980)

2 M. Grundner, J. Halbritter, J. Appl. Phys. 51, Oct. (1980)

3 W. Schwarz, J. Halbritter, J. Appl. Phys. 48, 4618 (1977)

4 A. Philipp, J. Halbritter, IEEE Trans. MAG-17, (1981)

5 A. Das Gupta, W. Gey, J. Halbritter, H. Küpfer, J.A. Yasaitis, J. Appl. Phys. 47, 2146 (1976)

6 J. Halbritter, Solid State Comm. 34, 675 (1980)

7 W. Schwarz, J. Halbritter, Proc. 4. Int. Conference on Solid Surfaces, Cannes, Sept. 1980; W. Schwarz, KfK-report-2913 (Kernforschungszentr., KfK ,1980)

8 H. Ekrut, A. Hahn, Frühjahrstagung der DPG, Freudenstadt, März 1980

9 J. Halbritter, Z. Phys. 266, 209 (1974)

10 J. Halbritter, KfK-Ext. 3/74-5 (Kernforschungszentrum Karlsruhe, 1974)

11 J. Halbritter, Proc. of Autumn School on Metal Physics, Piechowice (Poland) Nov. 1979

12 Tadashi Yogi, thesis (Cal Tech, Pasadena, 1977)
Guy Petterson, Hugo Parr, Phys. Rev. B 19, 3482 (1979)

13 P. Kneisel, O. Stoltz, J. Halbritter, Low Temperature Physics - LT 13 (Eds. E. Timmerhaus et al, Plenum Press, 19) Vol. 3, p. 202

14 Sh. Noguchi, Y. Kojima, J. Halbritter, submitted Nucl. Inst. Meth.

15 J. Halbritter, IEEE Trans MAG-11, 427 (1975) and
J. Halbritter, IEEE Trans. MAG-17, (1981)

16 J. Halbritter, Z. Phys. B 31, 19 (1978)

17 J. Halbritter, private communication

18 C.M. Lyneis, J.P. Turneaure, IEEE Trans MAG-13, 339 (1977);
H. Padamsee, this workshop

19 J. Halbritter, J. Appl. Phys. 41, 4581 (1970) and KfK-Ext. 2/69-6 (Kernforschungszentrum Karlsruhe 1969)

20 B. Piosczyk, P. Kneisel, O. Stoltz, J. Halbritter, IEEE Trans. NS-20, 108 (1973)

21 J. Halbritter, Proc. 72 Appl. Superconductivity Conference, Anapolis (IEEE, New York, 1972), p. 662

22 J. Halbritter, KfK-report 3/78-1 (Kernforschungszentrum Karlsruhe, 1978)

23 e.g. H.J. Fitting, H. Glaefeke, W. Wild, phys. stat. solidi A43, 185 (1977)

24 B.L. Henke, J. Liesegang, St.D. Smith, Phys. Rev. B 19, 3004 (1979)

25 H.J. Fitting, H. Glaefeke, W. Wild, Surf. Sci. 75, 267 (1978)

26 D.H. Anston, S. McAfee, C.V. Shank, E.P. Ippen, O. Teschke, Solid-State Electronics 21, 147 (1978); D. von der Linde, J. Kühl, H. Klingenberg, Phys. Rev. Lett. 44, 1505 (1980

27 J.W. Gadzuk, Phys. Rev. B1, 2110 (1970)

28 W.W. Dolan, W.P. Dyke, Phys. Rev. 95, 327 (1954)

29 M.J.G. Lee, R. Reifenberger, Surface Science 70, 114 (1978)
R. Reifenberger, private communication

30 N. Hilleret, private communication

31 K. Yoshida, M. Yoshioka, J. Halbritter, IEEE Trans. NS-26, 4114 (1979)

32 C.M. Lyneis, this workshop

33 H. Piel, this workshop

34 H.A. Schwettman, J.P. Turneaure, R.F. Waites, J. Appl. Phys. 45, 914 (1974)

35 J. Halbritter, Part. Acc. 3, 163 (1972)

36 J. Halbritter, P. Kneisel, to be published